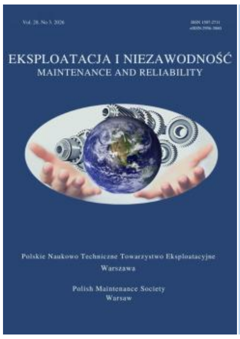

Eksploatacja i Niezawodnosc – Maintenance and Reliability

Volume 28 (2026), Issue 2

journal homepage: http://www.ein.org.pl

Article citation info:
Huang C, Xie J, Meng L, A New Lightweight Image Coding Method and Its Application in DC-DC Converter Parametric Fault Diagnosis, Eksploatacja i Niezawodnosc – Maintenance and Reliability 2026: 28(2) http:/10.17531/ein/216107

A New Lightweight Image Coding Method and Its Application in DC-DC Converter Parametric Fault Diagnosis

Indexed by: Web of Science Group

Chuangmian Huang[a,b], Linghui Meng[b,*] Jinyang Xie[c,*],

[a] Xidian University, Xian 710126, China
[b] School of Electromechanical Engineering, Guangdong Poly-technic Nomal University, Guangzhou, China
[c] School of Electrical Engineering, Beijing Jiaotong university, China

Highlights

- Use the experimental setting directly reflect the degradation process.
- A lightweight fault coding method is constructed.
- Reduced diagnosis time by 30%.

Abstract

A novel data encoding method that integrates Variational Mode Decomposition (VMD) with a new lightweight image coding technique is proposed and applied to the parametric fault diagnosis of DC-DC converters. This approach addresses the limitations of existing fault diagnosis methods, specifically the low diagnostic accuracy and poor noise resistance resulting from inadequate feature extraction. Initially, the parameter fault data of the DC-DC converter is decomposed into multiple modal components using the VMD method. Subsequently, these modal components are processed through Parameter-Weighted Trigonometric Difference (PWTD) coding to emphasize fault features. The enhanced features are then transformed into grayscale images, converting them into two-dimensional datasets for training the diagnostic model. Experimental results demonstrate that the proposed VMD-PWTDIC method achieves a diagnostic accuracy of 99.37%, which is 58.67% higher than four other comparative methods. Furthermore, compared to other methods, the proposed method reduces processing time by an average of 10.25 seconds. Additionally, the VMD-PWTDIC method exhibits superior performance in scenarios involving small sample sizes and noisy environments.

Keywords
DC-DC Converter, parametric fault, feature extraction, image coding

1. Introduction

With advancements in power electronics technology, electronic circuit systems are increasingly characterized by high-speed, integrated, large-scale, and complex components [1]. In aerospace, industrial automation, and various consumer products, the safe and stable operation of DC-DC converters is crucial for the reliability of power electronic equipment [2]. Given that DC-DC converters operate in complex and dynamic environments over extended periods, their operating states frequently change. This variability makes capacitors in DC-DC converters particularly susceptible to degradation, which can impair the normal functioning of the converter and potentially compromise the safety of power electronic equipment.

DC-DC converter failures are generally categorized into two types: Structural Hard Faults (SHFs) and Parametric Soft Faults

(*) Corresponding authc
E-mail addresses: C. Huang (ORCID: 0000-0002-0190-0620) huangchuangmian@163.com, L.Meng, (ORCID: 0000-0001-5915-4395) 13810476488@163.com, J. Xie (ORCID: 0009-0005-5507-6525) xjy19980920@163.com

(PSFs) [3]. SHFs typically result in a complete loss of circuit functionality, which cannot be recovered. Diagnosing SHFs is a reactive measure undertaken after a failure occurs, significantly impacting the safe and stable operation of the power system [4]. SHFs are often preceded by PSFs. When a PSF occurs, component parameters in the DC-DC converter deviate, but the circuit structure remains unchanged, leading to abnormal or degraded circuit functional specifications [5]. Therefore, accurate diagnosis of PSFs in DC-DC converters is vital for maintaining their reliability.

Existing fault diagnosis methods for DC-DC converters are primarily categorized into model-based methods, signal-based methods, and data-driven methods [6]. Among these, data-driven methods are particularly well-suited for fault diagnosis of DC-DC converters due to their superior generalization and diagnostic efficiency. The key to utilizing data-driven methods for diagnosing faults in power electronic circuits lies in effectively extracting features from signals that can accurately characterize faults [7]. These extracted features are then classified by a classifier to achieve precise fault diagnosis [8].

Commonly used feature extraction methods typically focus on obtaining time-domain, frequency-domain, or time-frequency-domain features from the signals. Techniques such as wavelet transform [9-10], variational mode decomposition [11-12], empirical mode decomposition [13-14], integrated empirical mode decomposition [15-16], and Hilbert transform [17] are often employed for this purpose. The features extracted through these methods are input into a classifier to identify the fault type. X.W. Wang et al. [18] proposed a lightweight damage identification framework based on an optimized Extreme Learning Machine . This framework extracts frequency features of vibration signals by integrating Empirical Mode Decomposition and optimizes the model weights of ELM using meta-heuristic algorithms. Experimental results demonstrated the efficiency and accuracy of the proposed method in the field of structural health monitoring.

However, traditional classifiers often rely heavily on expert knowledge in specific fields, and training classifiers solely with existing data can result in limited fault diagnosis accuracy.

Convolutional Neural Networks (CNNs), as a type of weight-sharing intelligent diagnostic tool, possess strong feature extraction capabilities and do not rely on expert knowledge, offering better generalization. Depending on the form of input data, CNNs can be categorized into one-dimensional CNNs (1DCNNs) and two-dimensional CNNs (2DCNNs). Y.Y. Zhao et al. [19] fed raw one-dimensional fault signals into a multi-branch 1DCNN for multi-scale feature extraction and utilized an attention mechanism to obtain the importance weights of feature maps learned by different 1DCNN branches. Experimental results demonstrated the effectiveness of this method in fault diagnosis. However, due to the need for large amounts of samples for training diagnostic models, when the original data is limited, the quality of generated data is low and cannot match real data, leading to poor diagnostic performance. Z. Jia et al. [20] combined Convolutional Neural Networks with deep bidirectional Long Short-Term Memory (LSTM) networks, enabling the model to achieve excellent performance even with insufficient training data. The robustness and generalization of the model were validated on two public datasets. B.Y. Song et al. [21] optimized the hyperparameters of the bidirectional LSTM network using Particle Swarm Optimization (PSO) and then fed the raw feature data into the optimized network to extract high-dimensional and time-correlated features from the signals, addressing the issue of model training and fault diagnosis under conditions of scarce samples. However, the performance of the diagnostic model heavily depends on the optimization algorithm's search efficiency, making its reliability uncertain, and its diagnostic performance in noisy environments unsatisfactory.

To enhance the model's noise resistance, Z.J. Zhang et al. [22] replaced the soft threshold function in the Deep Residual Shrinkage Network with an adaptive leakage threshold-based shrinkage function, achieving precise fault diagnosis even under high environmental noise. J.Y. Tong et al. [23] designed an improved pseudo-soft threshold function to eliminate signal distortion caused by the original soft threshold function and constructed an improved residual shrinkage unit using pseudo-soft threshold blocks and adaptive slope blocks, realizing fault diagnosis of rolling bearings under two different operating conditions in noisy backgrounds. This approach improved the robustness of the diagnostic model. However, due to the inherent high computational cost of the Deep Residual Shrinkage Network, its diagnostic efficiency is relatively low, and its diagnostic performance is unstable when the data volume is small. Additionally, Z. Jia et al. [24] extracted time-frequency domain features from signals using the S-transform and designed a sequential and excitation network attention module to assign weights to different channels. Faults were diagnosed precisely using the Swin Transformer. The effectiveness of the proposed method was verified in the context of intermittent fault diagnosis in power electronic systems. S.D. Wang et al. [25] designed a multi-channel spatiotemporal encoder that employs two independent graph multi-head attention neural networks to separately extract temporal features and multivariate spatial features. The extracted features are then integrated with a multi-head self-attention module, achieving precise extraction of UAV fault characteristics and effectively ensuring the reliability of UAV flight operations.

The diagnostic accuracy of 1DCNN is highly dependent on the characterization of fault features within the feature data. However, it is challenging to utilize spatial features from one-dimensional data effectively. To address this, image coding methods have been employed to represent spatial features of fault signals in a structured form. Converting one-dimensional fault data into images for use as 2DCNN training data has emerged as a promising solution in the field of fault diagnosis. J.S. Yang et al. [26] employed adversarial networks to learn the data distribution of real samples, generating new samples with similar distributions through adversarial training of generators and discriminators. These generated samples were then converted into grayscale images and used as input data for training a 2DCNN diagnostic model, achieving bearing fault diagnosis with limited samples. Peng W. et al. [27] proposed an improved alternate transfer learning method, which involved converting one-dimensional signals into grayscale images for diagnostic model input. This approach addressed feature transfer adaptation under varying operational conditions and across different bearing conditions. The direct conversion of one-dimensional data into grayscale images offers the advantages of smaller image size and faster model training. However, grayscale images exhibit limited capability to express features in noisy conditions, leading to poor noise resistance of the diagnostic model. L.L. Xue et al. [28] transformed fault signals into time-dependent Markov Transfer Field (MTF) images and introduced a self-calibrated coordinate attention mechanism to extract positional and feature channel information from these images, enabling accurate fault diagnosis under varying conditions. J.C. Song et al. [29] encoded fault signals using both Gramian Angular Field (GAF) and MTF methods. After converting one-dimensional signals into feature images, they fused these images using weighted least squares image fusion technology to enhance the supplementary information of fault features. Y.K. Zhou et al. [30] employed recursive graphs (RP) to encode fault signals in friction systems and achieved accurate diagnosis in noisy environments using convolutional neural networks (CNNs). X.P. Liu et al. [31] decomposed bearing vibration signals using wavelet packet decomposition, constructing approximate and detail coefficients at various scales. By removing redundant components based on symmetry characteristics, they realized bearing fault diagnosis through residual networks.

While these image coding methods offer significant advantages in improving diagnostic accuracy, the generated feature images often have large volumes. Consequently, model training using these images requires deep networks to extract features, resulting in slower training and longer diagnosis times. Furthermore, effectively distinguishing fault features in DC-DC converter parameter faults remains challenging. Therefore, there is an urgent need to develop a small, lightweight image coding method with excellent feature expression capabilities and noise resistance to address the complex fault diagnosis problems associated with DC-DC converters.

Traditional feature extraction methods primarily focus on separating the various components of a signal and then selecting the components related to the feature for reconstruction. This approach aims to suppress noise and enhance fault features[32]. However, since fault data from DC-DC converters are typically time series signals, it is challenging to extract more representative fault features, particularly the spatial features within the signal, solely through signal decomposition. When traditional methods decompose the fault signal and encode it into an image format as input for a 2D CNN, the spatial features in the original data are not effectively extracted. Consequently, the effective application of features in image encoding is difficult, leading to low diagnostic accuracy.

To address this issue, this paper proposes a new image encoding method for DC-DC converter fault diagnosis: Parameter Weighted Trigonometric Differential Image Coding

(PWTDIC). This method is used as input data for a CNN to accurately diagnose faults in DC-DC converters by significantly representing the spatial features of fault signals after feature extraction. Initially, the voltage signal from a DC-DC converter measurement point is decomposed using VMD to preliminarily extract features from the signal. Subsequently, the extracted data is encoded through PWTDIC, and the encoded data is divided into training, test, and validation sets. The training and test sets are used to train the CNN and save the training weights. These weights are then loaded into a CNN model with the same structure, and the model’ s diagnostic performance is validated on the validation set. Experimental results demonstrate that this method offers high diagnostic accuracy and robustness, maintaining strong performance even with small sample sizes. The innovative contributions of this work are summarized as follows:

1) Experimental Design: This study focuses on the actual output voltage, collecting voltage data from four measurement points of a DC-DC Boost circuit. These data directly reflect the degradation process of electrolytic capacitors in the Boost circuit.
2) Feature Extraction: Given that fault data are often overwhelmed by noise, making it difficult to extract effective features, this study employs VMD to decompose the feature data, suppressing noise in the original voltage signals. Subsequently, PWTD is applied to extract meaningful features, enabling efficient capture of fault characteristics.
3) Grayscale Conversion: By implementing grayscale conversion, lightweight image encoding is achieved, which significantly enhances data processing efficiency. This approach is particularly suitable for applications requiring rapid response.
4) PWTDIC Implementation: The use of PWTDIC ensures comprehensive expression of fault features in the feature data. This allows for precise diagnosis of DC-DC Converter PSF using a simple CNN, while also reducing the required model training time.
5) Performance in Practical Applications: In real-world scenarios, especially those involving small sample sizes and high noise levels, traditional methods often perform poorly. However, the VMD-PWTDIC method demonstrates superior performance under these challenging conditions, showcasing strong adaptability and robustness to various types of noise. This addresses the limitations of existing methods and provides a novel solution for such issues.

The flowchart illustrating the proposed PSF diagnosis for DC-DC Converter, which combines VMD, PWTDIC, and 2DCNN, is presented in Fig.1.

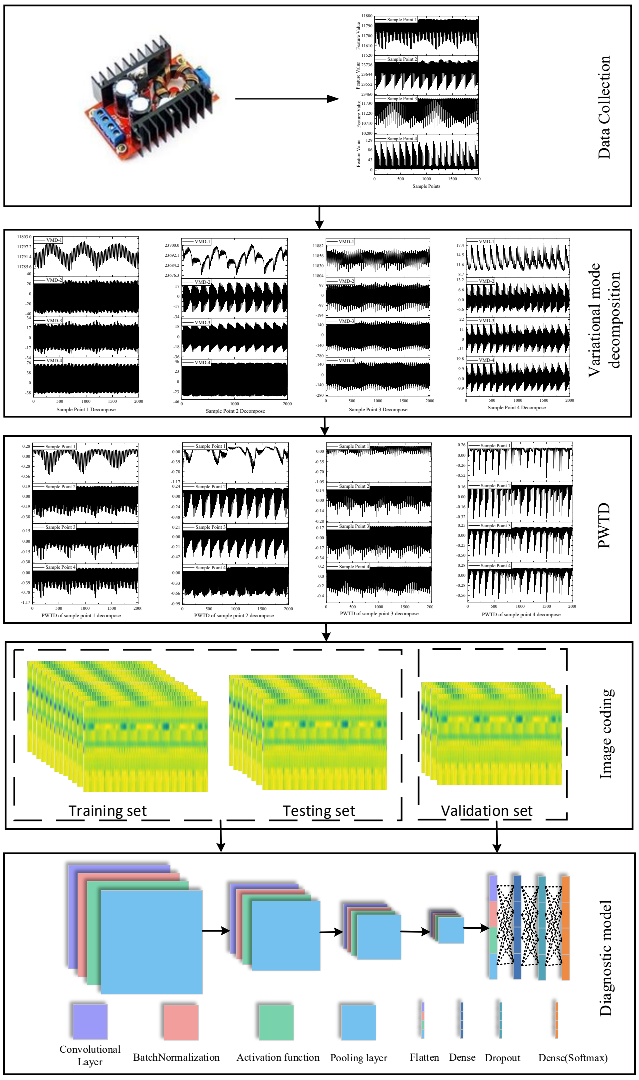

Fig. 1. shows the overall flow diagram of the proposed method.

2. Proposed method

The methodology can be segmented into three primary stages: feature extraction, image coding, and fault classification. Initially, the raw voltage data undergoes decomposition via VMD. Subsequently, the decomposed data is encoded into images using PWTDIC, constructing the fault dataset. This dataset is then partitioned into a training set, a test set, and a validation set. The training and test sets are utilized for model training within the 2DCNN framework, and the training weights are preserved. Following this, the retained training weights are integrated into a 2DCNN of the same architecture, and the model's diagnostic proficiency is validated on the validation set.

A. Variational Mode Decomposition

The VMD algorithm is an adaptive non-recursive modal decomposition method. This method utilizes the alternating direction method of multipliers (ADMM) algorithm to iteratively solve the constrained variational model, thereby obtaining the optimal solution for K intrinsic mode functions (IMFs) with center frequencies ω_k. The decomposition process of VMD can be summarized as follows:

Step 1: Initialization$\{\mu_k^1\}$, $\{\omega_k^1\}$, λ^1, $n \leftarrow 0$;

Step 2: Let $n = n + 1$, $k = k + 1$, update $\hat{\mu}_k^{n+1}$ and ω_k^{n+1} separately using equations (1) and (2). Stop iteration when $k = K$.

$$\hat{\mu}_k^{n+1}(\omega) = \frac{\hat{f}(\omega) - \sum_{i \neq k} \hat{\mu}_i^{n+1}(\omega) + \frac{\hat{\lambda}(\omega)}{2}}{1 + 2\alpha(\omega - \omega_k)} \quad (1)$$

Step 3: Update $\hat{\lambda}^{n+1}$ using the above equation:

$$\hat{\lambda}^{n+1}(\omega) = \hat{\lambda}^n(\omega) + \tau\left(\hat{f}(\omega) - \sum_k \hat{\mu}_k^{n+1}(\omega)\right) \quad (2)$$

Step 4: Given $\varepsilon > 0$, stop iteration when equation (3) is satisfied. Otherwise, repeat steps 2 to 4.

$$\varepsilon > \sum_k \frac{\|\hat{\mu}_k^{n+1} - \hat{\mu}_k^n\|_2^2}{\|\hat{\mu}_k^n\|_2^2} \quad (3)$$

The parameters K and α in the equation are preset parameters.

B. Parameter weighted trigonometric difference image coding

Due to the minimal differences between various faults indicated by DC-DC Boost circuit parametric fault data, traditional image coding methods struggle to extract significant fault features from this data. These methods often overlook the spatial features inherent in the fault data, making it challenging for diagnostic models to identify distinguishing features between different faults. To address this issue and enhance diagnostic accuracy, this paper proposes a Parameter Weighted Trigonometric Differential Image Coding (PWTDIC) approach. This method first scales the original feature data to extract the spatial information contained within it. The angular function values corresponding to the feature values are then weighted by the spatial information, and the resulting grayscale image is used as input for the diagnostic model. This approach aims to improve the accuracy of diagnosing parametric faults in the DC-DC Boost circuit.

The PWTDIC procedure is as follows:

a) For a given time series X = {x_1,x_2,⋯,x_n }, first, make all its values fall in the interval $[-1,1]$ by deflating them, as shown in eq.4.

$$\tilde{x}_i = \frac{(x_i - max(X)) + (x_i - min(X))}{max(X) - min(X)} \quad (4)$$

where x_i represents the original time series and $\tilde{x}_i$ represents the deflated time series. This normalization eliminates dimensional differences, ensuring stability in subsequent calculations.

Calculate the inverse cosine and arcsine values of the scaled feature data:

$$\theta_1 = ar\widetilde{ccos}\, x_i \quad (5)$$

$$\theta_2 = ar\widetilde{csin}\, x_i \quad (6)$$

By mapping the time series data into angular space through these trigonometric transformations, the non-linear expressiveness of the features is significantly enhanced. Additionally, this process effectively suppresses noise interference, improving the robustness of the feature representation.

b) The weighted parameters are derived using the inverse cosine and arcsine values. These parameters are then incorporated into the trigonometric difference formula, resulting in the parameter-weighted trigonometric difference formula:

$$PWTD = \frac{\theta_1}{\theta_1 + \theta_2} Cos(\theta_1) - \frac{\theta_2}{\theta_1 + \theta_2} Sin(\theta_2) \quad (7)$$

This step highlights the trends between adjacent points, further enhancing the distinguishability of fault features. The sensitivity of the method in capturing weak fault signals is significantly improved, making it effective even in noisy environments.

c) The output value obtained from PWTD is transformed into a grayscale image, which serves as the input data for the diagnostic model. By transforming the feature data into image form, local features can be automatically extracted through convolutional operations. This reduces reliance on manual feature selection while simultaneously improving the model's noise resistance.

3. 2D Convolutional Neural Network

CNN, a significant branch of deep learning, are inspired by the receptive field mechanism observed in biology[33]. CNNs propagate weight information between layers through local connections and global sharing mechanisms. They are widely used in various applications, including image classification, image segmentation, object tracking, and natural language processing[34]. A typical CNN architecture comprises several layers: convolutional layer, pooling layer, batch normalization layer, and an activation function layer. The convolutional layer consists of multiple convolutional kernels and biases for feature mapping. These kernels perform convolution operations on the feature tensor. The pooling layer reduces the dimensionality of features and computation time by extracting prominent features from a specified region, which also helps mitigate overfitting. The batch normalization layer normalizes the feature data by adjusting the mean and variance to 0 and 1, respectively, thereby ensuring that the data follows a normal distribution. The activation function layer introduces nonlinearity into the feature data through a nonlinear activation function, alleviating the problem of vanishing gradients during model training.

The structure of the 2D CNN model used in this paper is illustrated in Fig.2. The feature extraction component of the model is consisted of four convolutional blocks. Each block contains a convolutional layer, a batch normalization layer, an activation function layer, and a pooling layer. The number of convolutional kernels in these layers are 64, 128, 256, and 512, respectively, with each convolutional kernel having a size of 2. The pooling layer uses a pooling parameter of 2, and the nonlinear activation function employed is PreLU. After the original feature data is converted into feature images via PWTDIC, it is divided into training, testing, and validation sets with a ratio of 6:2:2. The training and testing sets are used to train the model. Upon completion of training, the model saves its feature weights. These weights are then loaded into a 2D CNN model with the same structure to validate the diagnostic performance of the model on the validation set, ultimately providing the diagnostic results for the parametric faults in the DC-DC Boost circuit.

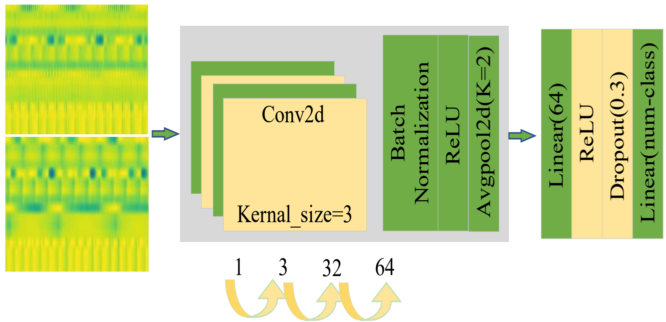

Fig. 2. 2DCNN model structure.

4. Circuit fault data

A Circuit structure and soft fault mode setting

To verify the performance of the proposed circuit fault diagnosis model, we built a boost circuit with 150 W power controlled by a UC3843 chip as an example. The input voltage of the circuit is 12 V, the output voltage is 24 V, the load is 100 Ω, the resistor power is 50 W, and the standard values of C1 and C5 are 1000 μF. The physical diagram, parameter failure test platform and circuit schematic are shown in Fig.3, Fig.4 and Fig.5, respectively.

In DC-DC circuits, the average failure rate of electrolytic capacitors is as high as 60%. Accordingly, we set up a study on the parameter failure of electrolytic capacitors C1 and C5 and classified the failure of their degradation degree into 16 types within the range of 10% to 50% of the nominal value of capacitance degradation, where f11 is the normal mode, f12, f13, f14 are C1 soft failures, f21, f31, f41 are C5 soft faults, and the rest are C1 and C5 for double soft faults, whose fault settings are shown in Table I.

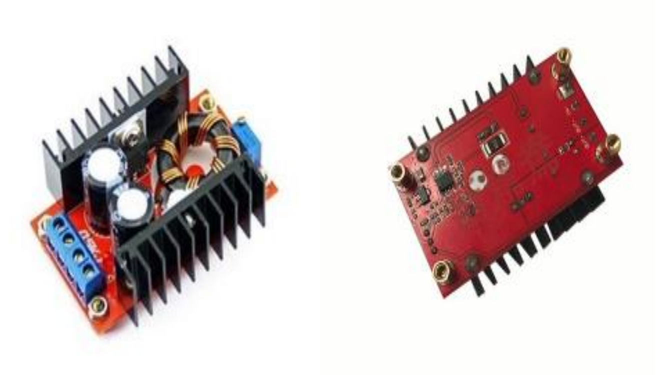
Fig. 3. 150W boost actual circuit diagram.

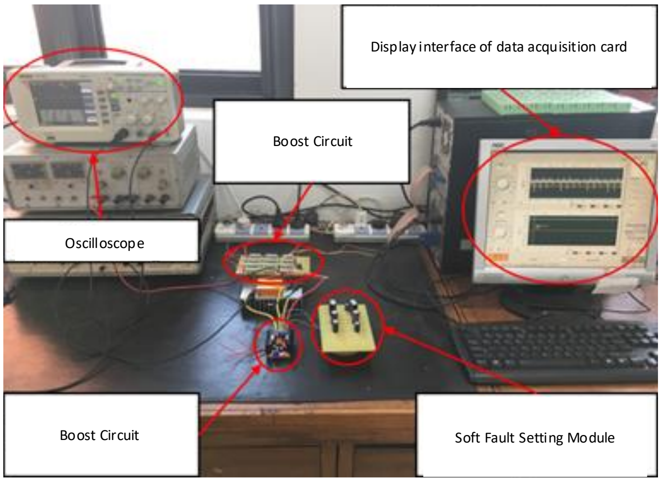

Fig. 4. 150W Boost Circuit Parametric Fault Test Bench.

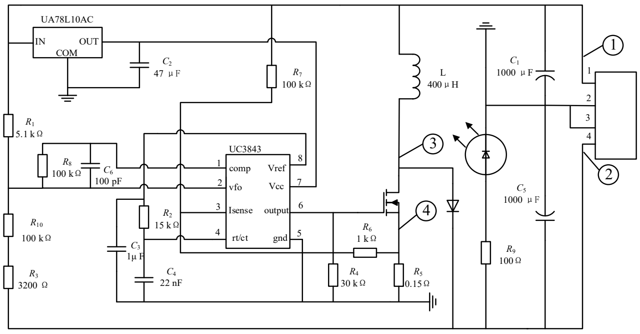

Fig. 5. 150W Boost circuit schematic.

Table 1. Capacitor fault model setting.

Capacitor type	C1/C5(μF)	Degradation degree of C1/C5 (%)	Fault category
F11	988/916	0~10/0~10	1
F12	988/887	0~10/10~20	2
F13	988/653	0~10/30~40	3
F14	988/554	0~10/40~50	4
F21	864/916	10~20/0~10	5
F22	864/887	10~20/10~20	6
F23	864/653	10~20/30~40	7
F24	864/554	10~20/40~50	8
F31	655/916	30~40/0~10	9
F32	655/887	30~40/10~20	10
F33	655/653	30~40/30~40	11
F34	655/554	30~40/40~50	12
F41	546/916	40~50/0~10	13
F42	546/887	40~50/10~20	14
F43	546/653	40~50/30~40	15
F44	546/554	40~50/40~50	16

B Analysis of measurement points

We used a PCI8335A data acquisition card to collect voltage at measurement points, where 1 measurement point-input voltage, 2 measurement points-output voltage, 3 measurement points-MOS tube drain voltage, and 4 measurement points-MOS tube source voltage all contain fault information of C1 and C5. Thus obtaining voltage signals of four measurement points can accurately represent the state of the circuit. Each measurement point has 2000 sampling points, and each fault state is sampled 50 times. The signal characteristics of the four measurement points are used as the basis for judging the soft fault category. Fig.8 shows the voltage waveforms of the four measurement points in the f33 fault mode.

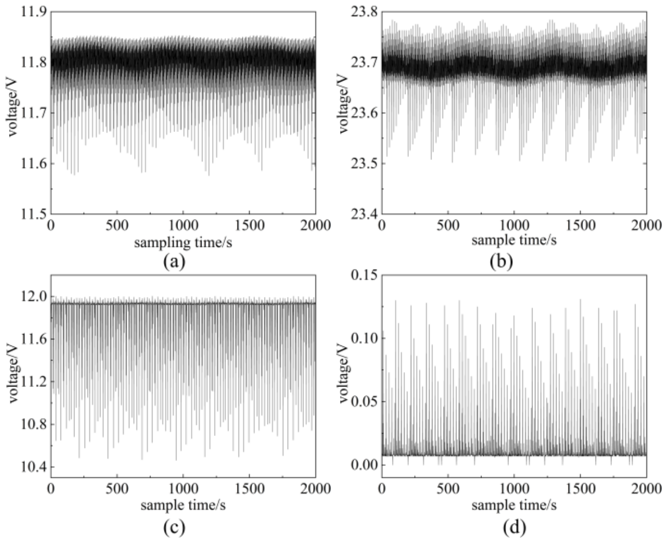

Fig. 6. Voltage signals: (a) Input voltage signal; (b) Output voltage waveform; (c) MOS tube drain voltage; (d) MOS tube source level voltage.

C Comparison of fault data processing results

The collected data from four measurement points, each corresponding to different fault types, were initially decomposed using VMD. The decomposed data were then further processed by Phase Weighted Transform Domain (PWTD) to extract features, which were subsequently converted into grayscale images for input into the diagnostic model. To illustrate the capability in extracting fault features of PWTD from the processed data more intuitively, we use the data from measurement point 1 of fault mode 1 (F11) as an example.

Fig. 7 to Fig. 9. shows the change process of the data of measurement point 1 in a noisy environment. It can be seen that the mode function which was generated by VMD is still affected by noise, so I can effectively extract the feature information therein, while after PWTD processing, the feature information in the data can be effectively extracted.

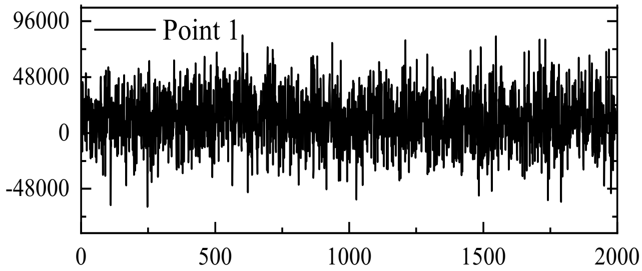

Fig. 7. Noise data at measuring point 1.

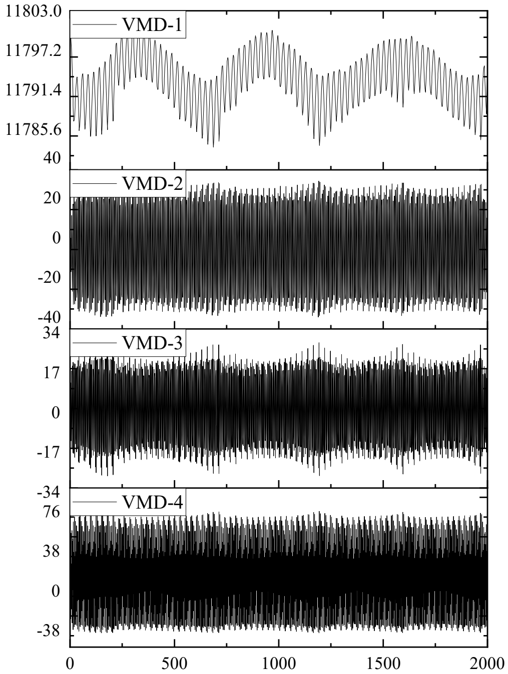

Fig. 8. Data after the VMD.

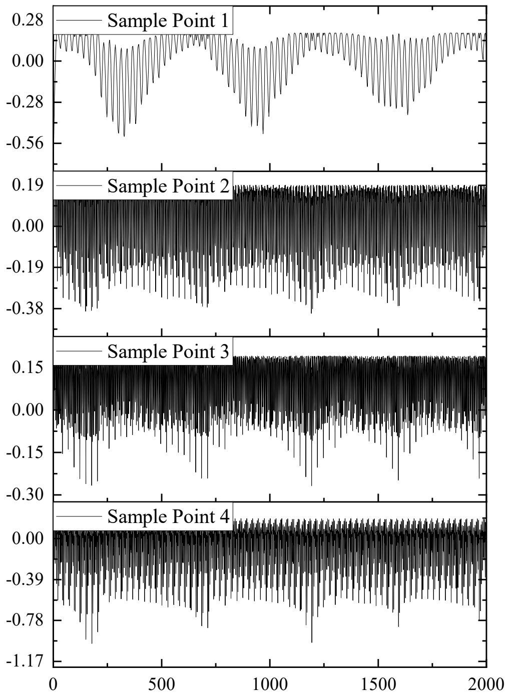

Fig. 9. Data after PWTD secondary processing.

The polar coordinate images of the data processed by different feature extraction algorithms, known as radar maps, are depicted. Fig.10 shows the radar map of the original data, Fig.11 displays the radar map of the data after decomposition by VMD, and Fig.12 presents the radar map of the data after further feature extraction using PWTD.

From Fig.10 to Fig.12, it is evident that the spatial features in the original data appear highly disorganized, making it challenging for the diagnostic model to effectively utilize these features. The radar map following VMD decomposition also indicates difficulty in extracting clear spatial features. However, after further extraction through PWTD, the spatial features in the data transform from chaotic to well-structured, demonstrating the effectiveness of PWTD in mining and elucidating the spatial features present in the data.

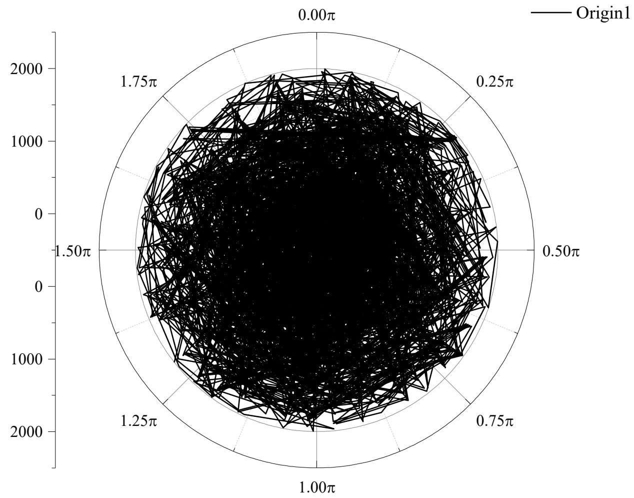

Fig. 10. Raw data radar map.

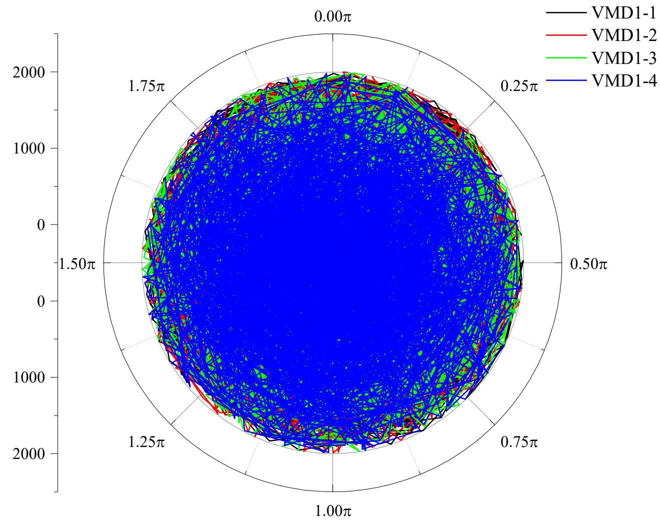

Fig. 11. VMD decomposition 4-layer radar map.

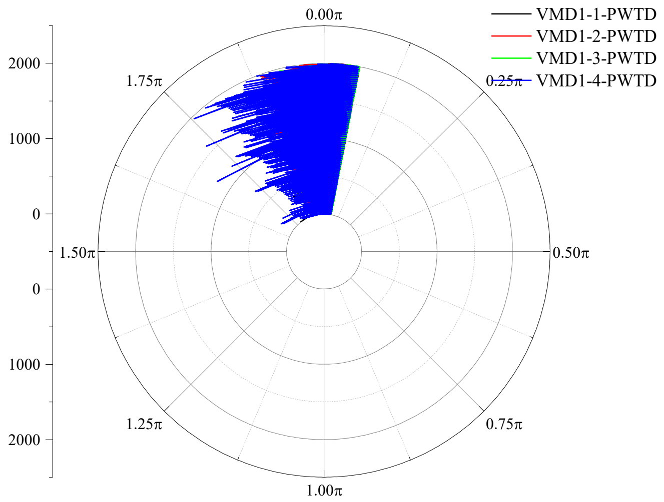

Fig. 12. PWTD radar diagram after VMD decomposition of 4 layers.

In addition, we plotted the four intrinsic mode functions (IMFs) obtained after VMD decomposition, as well as the corresponding radar images of the feature data following PWTD feature extraction, as illustrated in Fig.13 through Fig.16. The figures clearly demonstrate that the spatial features in the IMFs obtained after decomposition appear highly disordered. However, following further processing with PWTD, the spatial features in the data become more pronounced, with the features concentrating into a relatively narrow range.

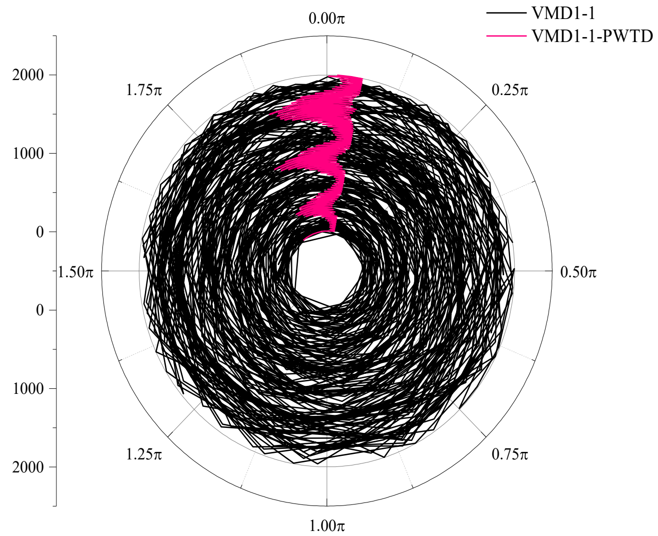

Fig. 13. Comparison of VMD1-PWTD radar charts-1.

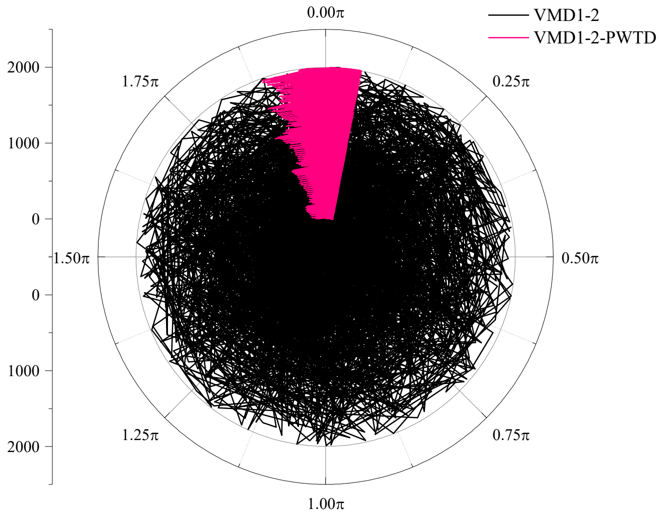

Fig. 14. Comparison of VMD1-PWTD radar charts -2.

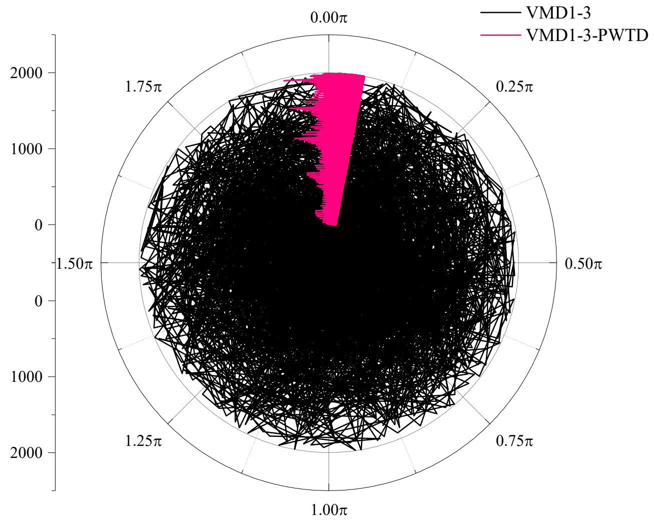

Fig. 15. Comparison of VMD1-PWTD radar charts -3.

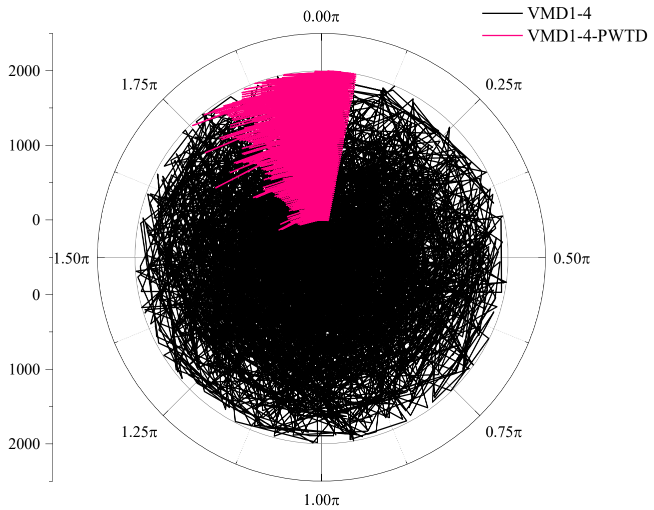

Fig. 16. Comparison of VMD1-PWTD radar charts -4.

Fig.17 displays the grayscale image generated after VMD-PWTD processing of data corresponding to 16 different faults in a DC-DC Boost circuit. To enhance the clarity of the image, we utilized a thermal map to improve its visibility during the image generation process.

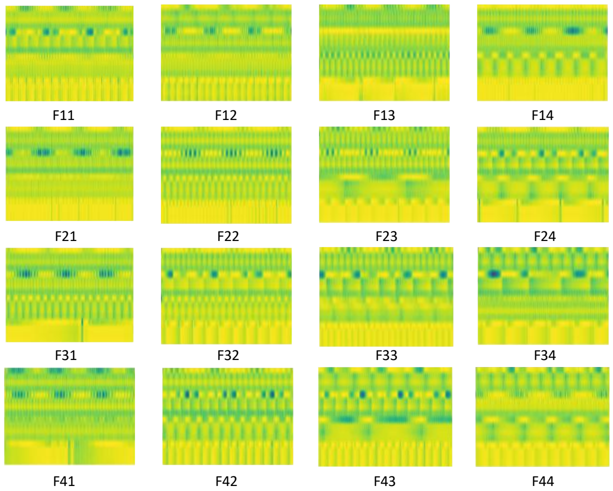

Fig. 17. 16 kinds of fault corresponding feature images.

5. Analysis of experimental results

In this section, the proposed diagnostic method is validated using the DC-DC Boost circuit parametric fault data described above. The software environment for the tests is a Windows 10 64-bit operating system with 128 GB of RAM, and the Pytorch framework is used on the PyCharm platform. The hardware environment includes an Intel® Xeon® Gold 6132 CPU and a Tesla V100-PCI-32GB GPU. The 2D CNN employed uses CrossEntropy as the loss function, Adam as the optimizer, and a learning rate of 0.001. Each experiment involves 100 training rounds on both the training set and the test set. The model weights from the round with the highest test accuracy are saved and then loaded to verify the diagnostic results on the validation set, yielding the final diagnostic accuracy.

The PWTDIC, GADF, GASF, RP, and MTF methods were used to encode the fault data decomposed by VMD. Each encoding process involved intercepting 2000 data points, with the interception frame translating by 1000 sampling points for each subsequent data capture. Consequently, 100 feature images were generated by each encoding method, The test set, training set and test set are divided according to the ratio of 6:2:2. The final diagnostic results for the different encoding methods are presented in Tab.2. Using PWTDIC for encoding, the diagnostic model achieved an accuracy of 99.37%, which represents an average increase of 58.67% compared to the other four image encoding methods. When the proportion of training data is reduced to 30%, meaning 18 feature images are used for training, the diagnostic accuracy of the proposed method remains at 96.87%, showing an average increase of 63.82% compared to the alternative methods. Furthermore, with only 6 training images, the proposed method achieves a diagnostic accuracy of 91.25%, which is an average improvement of 67.66% over the comparison methods. This demonstrates that the PWTDIC method exhibits excellent performance in parametric fault diagnosis for DC-DC Boost circuits and retains high feature extraction capability even with limited sample sizes.

Table 2. Experimental results of different coding methods and training scale.

		Accuracy	Precision	Recall	F1 Score
70% Train	PWTDIC	0.9937	0.9969	0.9970	0.9969
	GADF	0.3468	0.3469	0.3538	0.3346
	GASF	0.3562	0.3563	0.3502	0.3383
	RP	0.4843	0.4844	0.4699	0.4602
	MTF	0.4406	0.4406	0.4237	0.4220
30% Train	PWTDIC	0.9687	0.9638	0.9640	0.9637
	GADF	0.2406	0.2406	0.2430	0.2352
	GASF	0.3593	0.3594	0.3610	0.3209
	RP	0.4093	0.4094	0.3739	0.3661
	MTF	0.3125	0.3125	0.3228	0.2978
10% Train	PWTDIC	0.9125	0.9126	0.9204	0.9103
	GADF	0.1906	0.1906	0.1948	0.1793
	GASF	0.1843	0.1844	0.2040	0.1731
	RP	0.2750	0.2750	0.2866	0.2600
	MTF	0.2937	0.2938	0.2789	0.2621

It is important to note that PWTDIC directly converts the fault data waveform after PWTD into two-dimensional feature images without the need for complex image encoding technologies. Consequently, PWTDIC exhibits significant lightweight advantages compared to other methods. We compared the time required for the final verification stage across various methods, as shown in Tab.3. The diagnostic method proposed in this paper takes only 16 seconds, representing a maximum reduction of 15 seconds and an average reduction of 10.25 seconds compared to the other methods.

Table 3. Diagnostic time comparison.

	PWTDIC	GADF	GASF	RP	MTF
Times: s	16	31	30	21	23

Generally speaking, more complex feature image encoding methods result in larger feature image volumes and more complex diagnostic models for fault diagnosis. However, increased model complexity often leads to longer diagnostic times. Conversely, using a model with lower complexity may impair the effective extraction of fault features from complex feature images, resulting in lower diagnostic accuracy. For instance, when the feature images generated by the comparison method are used to train the diagnostic model proposed in this paper, the model shows higher training accuracy on the training set but performs poorly on the test set, leading to reduced diagnostic accuracy.

Fig.18 to Fig.22 illustrate the model training processes for PWTDIC and four comparison methods. As shown in Fig.19, the diagnostic model trained with feature images generated by PWTDIC achieves rapid convergence with high training and test accuracy, culminating in a diagnostic accuracy of 99.37% on the verification set. In contrast, while the four comparison methods yield high training accuracy on the training data, they exhibit low diagnostic accuracy on the test set and struggle to achieve good fitting.

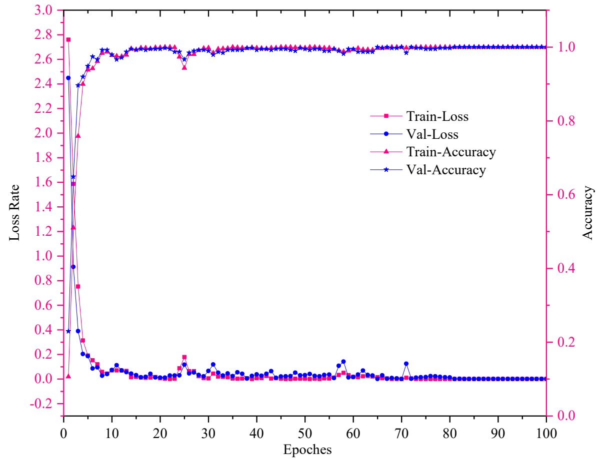

Fig. 18. Model training process when PWTDIC is used as input data.

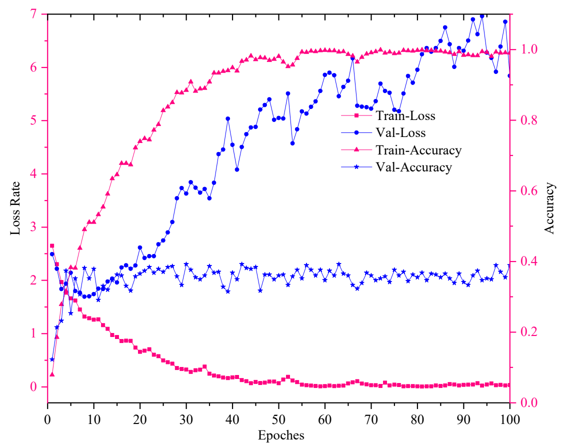

Fig. 19. Model training process when GADF is used as input data.

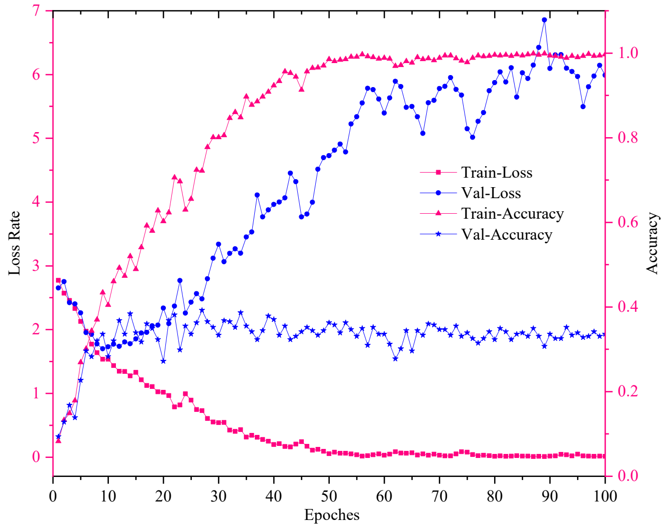

Fig. 20. Model training process when GASF is used as input data.

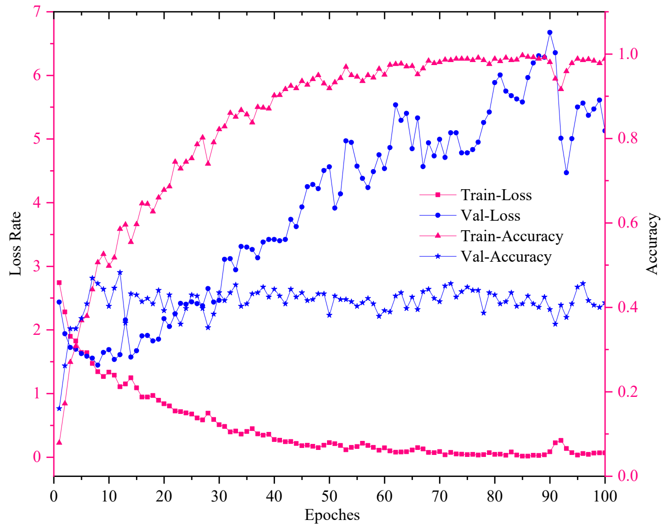

Fig. 21. Model training process when MTF is used as input data.

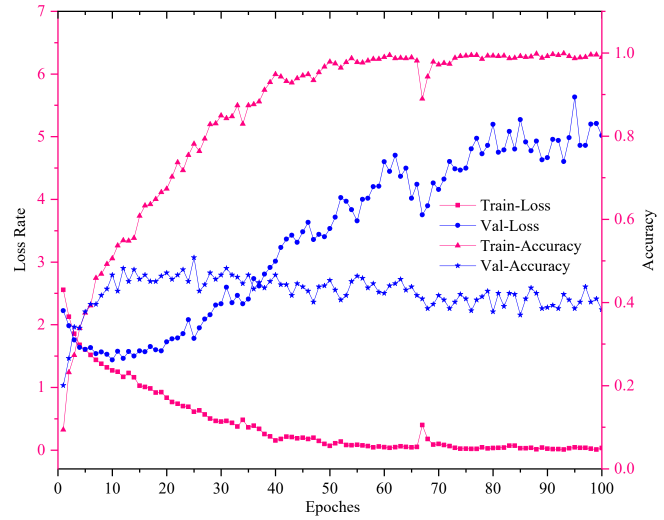

Fig. 22. Model training process when RP is used as input data.

In practical working conditions, data collection is often influenced by noise, which can obscure fault features and make them difficult for the diagnostic model to effectively extract. To assess the noise robustness of the diagnostic model proposed in this paper, white Gaussian noise of varying intensities was added to the original fault data to simulate real-world noise conditions. After performing feature extraction on the noisy data using VMD, the feature images were encoded with PWTDIC and four comparison methods, and the 2DCNN was used for diagnosis. The final diagnostic results are presented in Fig.23. With the addition of 6 dB Gaussian white noise to the fault data, the proposed method achieved a diagnostic accuracy of 99.79%, which is 92.83% higher than that of the other four methods. At noise levels of -6 dB and -12 dB, the proposed method maintained diagnostic accuracies of 98.75% and 97.81%, respectively, demonstrating clear advantages over the other four image encoding methods.

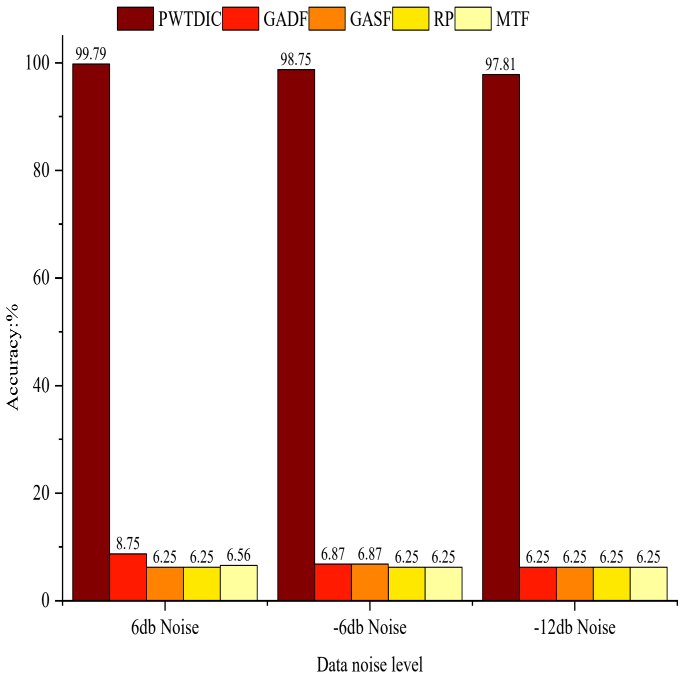

Fig. 23. Experimental results under different noises.

6. Conclusion

To address the challenges of feature extraction, low accuracy of image conversion methods, and prolonged diagnosis times in parametric fault diagnosis of DC-DC converters, this paper proposes a parametric fault diagnosis method for DC-DC converters based on VMD-PWTDIC. The proposed method begins by decomposing the original fault data using VMD into different IMFs. These IMFs are then encoded with PWTDIC, which maximizes the preservation of fault features within the IMF components. Additionally, PWTDIC employs grayscale images for feature data transformation, mitigating the issue of extended model diagnosis times caused by the large volume of feature images.

Experiments conducted on the DC-DC Boost parametric fault dataset demonstrate that the proposed method is effective for fault diagnosis. The diagnostic model achieved an accuracy of 99.37%, which is 58.67% higher than that of the four comparison methods. When using only 10% of the original dataset size to train the diagnostic model, the proposed method attained a diagnostic accuracy of 91.25%, representing an average improvement of 67.66% over the comparison methods. Moreover, the training process of the diagnostic model illustrates the advantages of the proposed method in terms of convergence speed. With the addition of -6 dB and -12 dB noise to the fault data, the diagnostic accuracy of the proposed method reached 98.75% and 97.81%, respectively, showing clear advantages over other coding methods. In terms of model diagnosis time, the feature images encoded by PWTDIC require only 16 seconds, which is an average reduction of 10.25 seconds compared to the four other image coding methods.

References

1. T. Zhang, T. Li, A novel approach of analog circuit fault diagnosis utilizing RFT noise estimation[J], Analog Integrated Circuits and Signal Processing, Vol.98, pp.517-526, March. 2019. https://doi.org/10.1007/s10470-018-1351-x
2. J. Zhen, Z.B. Liu, Z.W. Huang, et al. DC-DC Buck circuit fault diagnosis with insufficient state data based on deep model and transfer strategy[J], Expert Systems with Applications, Vol.213, Part A, pp.118918, March. 2023. https://doi.org/10.1016/j.eswa.2022.118918
3. Q. Sun, Y. Wang, and Y. Jiang, A novel fault diagnostic approach for DC–DC converters based on CSA-DBN[J], IEEE Access, Vol.6, pp.6273-6285, 2018. https://doi.org/10.1109/ACCESS.2017.2786458
4. Q.Z. Zhao, Y. Li, and S.Tian, et al. Condition Monitoring and Fault Handling Method Based on Big Data Analysis of Intelligent Distribution Network[J], Power System Technology, Vol.40, no.03, pp.774-780, 2016.
5. D. Binu, B.S. Kariyappa, A survey on fault diagnosis of analog circuits: Taxonomy and state of the art[J], AEU - International Journal of Electronics and Communications, Vol.73, pp.68-83,2017. https://doi.org/10.1016/j.aeue.2017.01.002

6. Y. Fu, Z. Gao, H. Wu, et al. Data-driven fault classification for non-inverting buck-boost DC–DC power converters based on expectation maximisation principal component analysis and support vector machine approaches[C], 2021 IEEE 1st International Power Electronics and Application Symposium (PEAS), pp.1-6, 2021. https://doi.org/10.1109/PEAS53589.2021.9628697
7. Q. Xue , B.Y. Xu , C.B. He, et al., Feature extraction using hierarchical dispersion entropy for rolling bearing fault diagnosis[J], IEEE Transactions on Instrumentation and Measurement, Vol.70, pp.1-11, Jun. 2021. https://doi.org/10.1109/TIM.2021.3092513
8. Y. Jiang, L. Xia, and J. Zhang, A Fault Feature Extraction Method for DC–DC Converters Based on Automatic Hyperparameter-Optimized 1-D Convolution and Long Short-Term Memory Neural Networks[J], IEEE Journal of Emerging and Selected Topics in Power Electronics, Vol.10, no.4, pp.4703-4714, Aug. 2022. https://doi.org/10.1109/JESTPE.2021.3131706
9. X.M. Tao, C. Ren, Y.K. Wu, et al. Bearings fault detection using wavelet transform and generalized Gaussian density modeling[J], Measurement, Vol.155, PP.107557, 2020. https://doi.org/10.1016/j.measurement.2020.107557
10. C. Liu, F. Zhuo and F. Wang, Fault Diagnosis of Commutation Failure Using Wavelet Transform and Wavelet Neural Network in HVDC Transmission System[J]. IEEE Transactions on Instrumentation and Measurement, Vol.70, pp.1-8, 2021. https://doi.org/10.1109/TIM.2021.3115574
11. H. Li, X. Wu, T. Liu, et al. Composite fault diagnosis for rolling bearing based on parameter-optimized VMD[J], Measurement, Vol.201, pp.11637, 2022. https://doi.org/10.1016/j.measurement.2022.111637
12. Z. Jin, D.Q. He, Z.X. Wei, Intelligent fault diagnosis of train axle box bearing based on parameter optimization VMD and improved DBN[J], Engineering Applications of Artificial Intelligence, Vol.110, PP.104713, 2022.
13. X. Qi, C.F. Hong, T. Ye, et al. Frequency reconstruction oriented EMD-LSTM-AM based surface temperature prediction for lithium-ion battery[J], Journal of Energy Storage, Vol.84, Part.B, PP.111001, 2024.
14. A. Redekar, H.S. Dhiman, D. Deb, et al. On reliability enhancement of solar PV arrays using hybrid SVR for soiling forecasting based on WT and EMD decomposition methods[J], Ain Shams Engineering Journal, Vol.15, Issue.6, pp.102716, 2024.
15. P. Zou, B.C. Hou, J. Lei, et al. Bearing Fault Diagnosis Method Based on EEMD and LSTM[J], International Journal of Computers Communications & Control, Vol.15, no.1, 2020. https://doi.org/10.15837/ijccc.2020.1.3780
16. T. Zhong, J.F. Qu, X.Y. Fang, et al. The intermittent fault diagnosis of analog circuits based on EEMD-DBN[J], Neurocomputing, Vol.436, pp.74-91, 2021. https://doi.org/10.1016/j.neucom.2021.01.001
17. R. S. Kumar, I. G. C. Raj, I. Alhamrouni, et al. A combined HT and ANN based early broken bar fault diagnosis approach for IFOC fed induction motor drive[J], Alexandria Engineering Journal, Vol.66, pp.15-30, 2023. https://doi.org/10.1016/j.aej.2022.12.010
18. X.W. Wang, Y.H. Zhao, Z.H. Wang, et al. An ultrafast and robust structural damage identification framework enabled by an optimized extreme learning machine[J], Mechanical Systems and Signal Processing, Volume 216, 2024, 111509, ISSN 0888-3270, https://doi.org/10.1016/j.ymssp.2024.111509.
19. Y.Y. Zhao, Y.G. He, Z.K. Xing, et al., Multibranch 1-D CNN Based on Attention Mechanism for the DAB Converter Fault Diagnosis[J], IEEE Transactions on Instrumentation and Measurement, Vol.71, pp.1-12, 2022. https://doi.org/10.1109/TIM.2022.3203445
20. Z. Jia, Z.F. Li, K. Zhao, et al. CNN-DBLSTM: A long-term remaining life prediction framework for lithium-ion battery with small number of samples[J], Journal of Energy Storage, Volume 97, Part B, 2024, 112947, ISSN 2352-152X, https://doi.org/10.1016/j.est.2024.112947.
21. B.Y. Song, Y. Liu, J.Z. Fang, et al. An optimized CNN-BiLSTM network for bearing fault diagnosis under multiple working conditions with limited training samples[J], Neurocomputing, Vol.574, pp.127284, 2024.
22. Z.J. Zhang, L. Chen, C.L. Zhang, et al. GMA-DRSNs: A novel fault diagnosis method with global multi-attention deep residual shrinkage networks[J], Measurement, Vol. 196, 2022, https://doi.org/10.1016/j.measurement.2022.111203.
23. J.Y. Tong, S.Y. Tang, Y. Wu, et al. A fault diagnosis method of rolling bearing based on improved deep residual shrinkage networks, Measuremen[J]t, Vol. 206, 2023, https://doi.org/10.1016/j.measurement.2022.112282.
24. Z. Jia, S.D. Wang, K. Zhao, et al. An efficient diagnostic strategy for intermittent faults in electronic circuit systems by enhancing and locating local features of faults, Measurement science and technology, Vol.35, no.3. 2024, doi: 10.1088/1361-6501/ad156f.
25. S.D. Wang, Z. Jia, Z.B. Liu, et al, Self-supervised contrast learning based UAV fault detection and interpretation with spatial‐temporal information of multivariate flight data[J], Expert Systems with Applications, Vol.267, pp.126156, 2025,
26. J. Yang, J. Liu, J. Xie, et al. Conditional GAN and 2-D CNN for Bearing Fault Diagnosis With Small Samples[J], IEEE Transactions on

Instrumentation and Measurement, Vol.70, pp.1-12, 2021. https://doi.org/10.1109/TIM.2021.3119135
27. P. Wang, D.Q. Li, H. Wang, Rolling bearing fault diagnosis algorithm based improved alternating transfer learning, Journal of vibration and shock[J], Journal of Vibration and Shock, Vol.43, no.5, pp.239-249, Jun. 2024.
28. L. Xue, C. Lei, M. Jiao, et al. Rolling Bearing Fault Diagnosis Method Based on Self-Calibrated Coordinate Attention Mechanism and Multi-Scale Convolutional Neural Network Under Small Samples[J], IEEE Sensors Journal, Vol.23, no.9, pp.10206-10214, May. 2023. https://doi.org/10.1109/JSEN.2023.3260208
29. J. Song, X. Wu, L. Qian, et al. PMSLM Eccentricity Fault Diagnosis Based on Deep Feature Fusion of Stray Magnetic Field Signals[J], IEEE Transactions on Instrumentation and Measurement, Vol.73, pp. 1-12, 2024. https://doi.org/10.1109/TIM.2023.3346539
30. Y.K. Zhou, R. Zhu, H. Zhao, et al. Influence of noise on wear fault diagnosis based on recurrence plot[J], Measurement, Vol.205, pp.112158, 2022.
31. X. Liu, L. Xia, J. Shi, et al. A Fault Diagnosis Method of Rolling Bearing Based on Improved Recurrence Plot and Convolutional Neural Network[J], IEEE Sensors Journal, Vol.23, no.10, pp.10767-10775, May. 2023. https://doi.org/10.1109/JSEN.2023.3265409
32. X.C. Luan, Z.P. Zhang, Y.D. Shan, et al, Main bearing fault feature enchancement method based on optimal variational mode decomposition and computational order analysis[J], Journal of propulsion technology, pp.1-13, Jun. 2024,
33. T. Guo, L.P. Wu, C.J. Wang, et al. Damage detection in a novel deep-learning framework: a robust method for feature extraction[J], Struct. Health Monit. Vol.19, no.2, pp.424–442, 2020. https://doi.org/10.1177/1475921719846051
34. X.P. Qiu, “Neural Networks and Deep Learning,” China Machine Press, 2019.